Received: Added at production | Revised: Added at production | Accepted: Added at production

DOI: xxx/xxxx

RESEARCH ARTICLE

Numerical analysis and design of a high-frequency surface acoustic wave transducer: influence of piezoelectric substrates and IDTs configurations

Alonso Fernandez-Garcia[1] | **Veronica Irais Solis-Tinoco**[2] | **Miguel Angel Aleman Arce**[2] | **Luis Alfonso Villa-Vargas**[2] | **Marco Antonio Ramírez Salinas**[2] | **Juan Carlos Sanchez Garcia**[1]

[1]Grupo de microelectronica aplicada, Escuela Superior de Ingeniería Mecánica y Eléctrica - Culhuacán,IPN, CDMX, Mexico

[2]Laboratorio de sistemas embebidos, Centro de Investigaciones en Computación,IPN, CDMX, Mexico

Correspondence
Veronica Irais Solis-Tinoco, Centro de Investigaciones en Computación, Instituto Politecnico Nacional, CDMX 07738, Mexico.
Email: irais.solis@cic.ipn.mx

Abstract

The development of SAW transducers requires a series of steps ranging from material selection, geometry design, as well as, the selection of fabrication techniques for their characterization and validation process. Here, we use the finite element method in COMSOL Multiphysics to present a methodology and a detailed analysis of the design of a SAW transducer in a delay line configuration. First, we simulate single-finger and double-finger configurations of IDTs on LiNbO3 in 64°YX and LiNbO3 128°YX orientation, with the objective of 1) comparing the simulation results with the analytical delta model to validate the simulation process, presenting Pearson correlation values ranging from 0. 76 to 0.84. 2) calculate a maximum frequency value obtainable for those configurations from a resolution of 5 microns in the photolithography technique, used for the fabrication of SAW transducers. Next, we extended the analysis to study a specific transducer design made to operate at a resonant frequency of 97 MHz. In order to determine the influence of piezoelectric material and IDT configuration we compared identical designs on 128°YX and 64°YX orientations of LiNbO3 with single and double finger configurations and adding the SPUDT configuration. We observed the best results for the single-finger IDT configuration in 128°YX LiNbO3 orientation compared to the other variants through its insertion loss level of -7.29 dB, its average sidelobe level of 18.63 dB, and its average transition band slope for the main lobe of 119.59 dB/MHz. The results obtained can serve as a guide for new researchers or students to expand the use of numerical tools in the design of SAW transducers and SAW devices.

KEYWORDS
SAW, Design, Numerical simulation, Piezoelectric cut orientation, Interdigitated transducer, COMSOL, ultrasonic transducer,

1 | INTRODUCTION

There are many electronic devices such as filters[1], oscillators, ultrasonic transducers[2,3], etc. that are made of piezoelectric materials and are present in much of today's technology. In particular, the use of piezoelectric transducers extends from the manufacture of sensors for pressure, temperature, humidity, viscosity, gases, and even in novel biosensing platforms.[4,5,6,7]. Within the classification of piezoelectric filters and transducers, there are some so-called surface acoustic wave devices (SAW transducers/filters) that are based on the generation and reception of acoustic waves by interdigitated transducers (IDT) usually made of metallic thin films deposited on the surface of a piezoelectric material.

The design of the IDTs in a SAW transducer focuses on meeting the user's requirements for the value of the resonant frequency, levels of insertion loss, side lobe levels, and slope of the transition band. The IDTs are designed taking into account the basic properties of the piezoelectric material. A wide variety of materials can be selected, such as Quartz, ZnO, AlN, LiTaO3, PZT, or LiNbO3. The choice is based primarily on the mode of vibration that the crystalline orientation inherits to the selected substrate,

for example, if a piezoelectric transducer is used in a gas sensor, any material that has a Rayleigh-type mode of vibration, such as ZnO or LiNbO3 in 128°YX orientation could be used. However, if the transducer is used in applications with the handling of liquid samples the Rayleigh-type vibration mode could cause high attenuation of the acoustic energy. Then, an orientation that allows a Shear-horizontal SAW (SH-SAW) mode to be obtained should be used e.g., Quartz, or LiNbO3 in 36°YX, 64°YX[8] orientation. The design of a SAW transducer can be focused on satisfying a specific frequency response that can be modeled using different tools such as transverse filter theory, equivalent circuit theory, mode-coupling theory, or delta model[9,10]. Despite all the modeling tools available, there is a growing interest in the use of numerical simulations to be a complementary tool in SAW transducer design due to the possibility to represent the anisotropic properties of the materials and to simulate the physical interactions of the device with its environment, as well as to represent complex geometries of the IDTs or to study the effect of manufacturing variations, all of these tasks can be very complex if an analytical solution is desired.[11,12,13] In this work, we made a comparative analysis of a SAW transducer design with LiNbO3 in 64°YX and 128°YX orientation and three different IDT configurations; 1) single, 2) double finger, and 3) single-phase unidirectional transducer (SPUDT). The analysis was performed using COMSOL Multiphysics to study the variation in the frequency response of the SAW transducers. The simulation results were compared with an analytical model to validate the process and then the simulation was extended to design a SAW transducer operating at a resonant frequency of 97 MHz. The present analysis demonstrates that numerical modeling is a valuable process for any SAW transducer's rapid design and microfabrication cost reduction.

2 | SAW TRANSDUCER DESIGN

We design and analyze a SAW transducer in a delay line configuration that consists of two ports, see Figure 1, an input, and an output port, with aluminum IDTs whose connection to any external equipment is made through bonding pads, these IDTs are separated by a distance *l* which determines the delay time between the ports, the attenuation, and the changes in the phase of the signal. The design consists of two principal parts: piezoelectric material selection and the IDT design as described below.

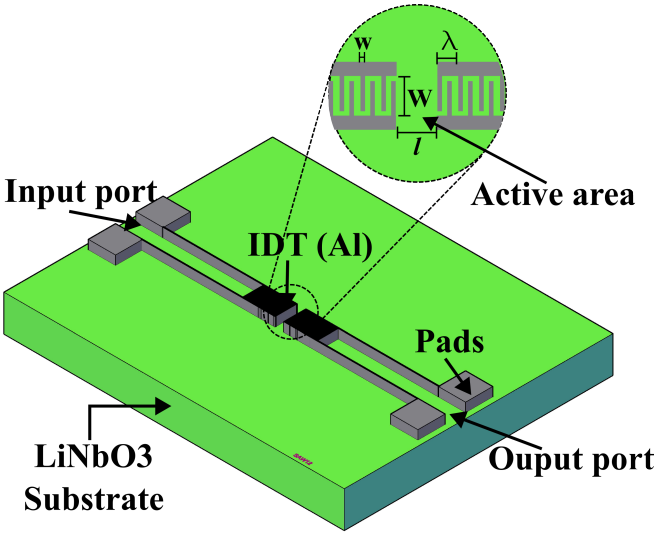

FIGURE 1 SAW transducer in delay line configuration. The metallic aluminum structures deposited on the piezoelectric surface define the IDT geometries with fingers of width (w) and overlapped by a distance (W) called acoustic aperture, each IDT form one of the two ports one input and one output separated by a distance *l* that define the active area, that could be used in sensing applications.

2.1 | Piezoelectric material

The piezoelectric material selection is oriented to maximize the efficiency of transduction of surface acoustic waves, this is achieved by the correct choice of the piezoelectric material that has a high electromechanical coupling factor (k), high propagation velocity (V_f), and the existence of a particular vibration mode (Raylegh, SH-SAW, etc.). The LiNbO3 is a material with a trigonal 3m crystal structure, in the 128°YX orientation shows a Raylegh-type vibration mode, a piezoelectric coupling factor $k^2 = 0.055$, a relative piezoelectric permittivity value of $\epsilon_p = \epsilon_0 \times 56$ and a propagation velocity $V_f = 3975$ m/s. On the other hand, in the 64°YX orientation, the vibration mode is SH-SAW type and shows slightly different values from the previous orientation having a piezoelectric coupling factor $k^2 = 0.113$, a relative piezoelectric permittivity value $\epsilon_p = 52 \times \epsilon_0$ and propagation velocity $V_f = 4742$ m/s [14].

The description of the LiNbO3 and consequently of the SAW transducers piezoelectric nature is generally made using the piezoelectric constitutive equations (1) and (2) that show fundamental information about the anisotropic nature of the physical problem and that can help to correctly set the physical problem in the COMSOL simulation for transducers design.

$$T = c_E \cdot S - e^t \cdot E \tag{1}$$

$$D = e \cdot S - \epsilon_s \cdot E \tag{2}$$

where T is the vector of stress components, c_E is the matrix of stiffness coefficients under constant electric field, S is the vector of the strain components, E is the vector of electric field components, D is the vector of electric charge displacement components, e is the matrix of piezoelectric coupling coefficients, and ϵ_s the matrix of electric permittivity considered under constant stress [15].

2.2 | Interdigital transducers design

We have divided the IDT design into two parts. First, SAW transducers for the single-finger and double-finger IDT for both LiNbO3 orientation (see Figure 2a,b) were designed by extracting the main geometrical parameters, estimated for a desired level of insertion loss (IL). These two IDT configurations are very similar in design but with slight differences that can become significant in the fabrication process of high-quality devices. The single-finger configurations are easier to fabricate under a low-definition photolithographic process because, in this configuration for a desired equivalent wavelength (λ_s), the relationship $\lambda_s = 4w$ is met, then we have wider fingers, unlike in the dual-electrode configuration where the equivalent acoustic wavelength (λ_d) meets the relationship $\lambda_d = 8w$. For this designs, all the geometrical parameters: finger width (w), acoustic aperture (W), separation ports (l), number of fingers (N), and equivalent acoustic wavelength (λ) were obtained following a similar process as in Cole et. al. [16] or Soluch et. al. [17] but with the objective of obtaining a design criterion based on the maximum achievable resonance frequency, using the maximum resolution (5 μm) of the photolithography technique available to us. The geometric parameters of the designed SAW transducer obtained are shown in Table 1. These are validated by comparing them with the analytical delta model, a process that at the same time allows to validate the numerical simulations so that from these results we can extend the analysis to more complex designs with the advantage of being able to take into account physical effects such as multiple reflection and attenuation effects, for which their study with analytical models can be too complicated.

For the validation we use the delta analytical model, which considers the IDTs as a periodic arrangement of N pairs of fingers, then the electrical excitation at each port in the SAW transducer is the contribution of N electrical potential sources, from the delta model a voltage transfer function can be extracted as in K. Hashimoto's reference [18] from which the dispersion parameter S21 is calculated.

$$S21 = \frac{-2y_{12}\sqrt{y_1 y_2}}{-y_{12}y_{21} + (y_1 + y_{11})(y_2 + y_{22})} \tag{3}$$

Here y_1 and y_2 are the source and load admittances, y_{11} and y_{22} are the input and output port IDT admittance, y_{12} and y_{21} are the forward and backward transfer-admittance. From equation 3 the insertion loss (IL) of the device can be extracted, which is directly related to the S21 parameter through the equation 4

$$IL = -20\log[S21] \tag{4}$$

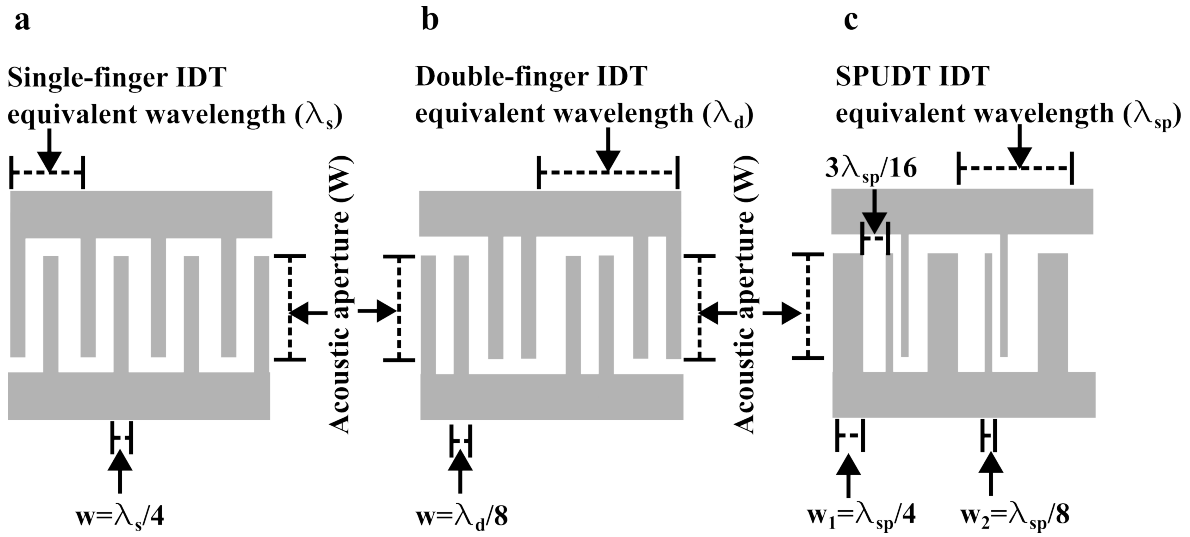

FIGURE 2 Single, double-finger and SPUDT configuration. The main geometrical difference between configurations is observed, the number of fingers per period where λ_s, λ_d and λ_{sp} are the equivalent acoustic wave of single, double electrode and SPUDT configuration, w is the finger width for the first two configurations but SPUDT haves two different finger sizes w_1 and w_2, also W is the acoustic aperture equivalent to the overlap distance between fingers of different polarity in the same IDT.

TABLE 1 Design parameters for single and double-finger configurations on LiNbO3 128°YX and LiNbO3 64°YX.

		Single IDT		Double IDT	
Piezoelectric	**Property**	**Abreviature**	**Value**	**Abreviature**	Value
128°YX LiNbO3	Finger width	w_s	5 μm	w_d	5 μm
	Acoustic wavelength	λ_s	20 μm	λ_d	40 μm
	Number of finger pairs	N_s	20	N_d	20
	Acoustic aperture	$100\lambda_s$	2 mm	$100\lambda_d$	4 mm
	Resonance frequency	f_s	194 MHz	f_d	97 MHz
	Ports separation	l_s	140 μm	l_d	280 μm
64°YX LiNbO3	Finger width	w_s	5 μm	w_d	5 μm
	Acoustic wavelength	λ_s	20 μm	λ_d	40 μm
	Number of finger pairs	N_s	20	N_d	20
	Acoustic aperture	$100\lambda_s$	2 mm	$100\lambda_d$	4 mm
	Resonance frequency	f_s	226 MHz	f_d	113 MHz
	Ports separation	l_s	140 μm	l_d	280 μm

Once the previous designs were validated and a design criterion for the maximum resonance frequency obtained was established, we began with second part in the IDT design, in which any IDT can be simulated and arbitrarily designed in other configurations such as the Single Phase Unidirectional Transducer (SPUDT) see Figure 2 c, which is a configuration that potentially reduces the triple transit signal in which the surface acoustic wave propagates only from one side of the transducer input port, giving low insertion loss values, it has two different sizes of finger width $w_1 = \lambda_{sp}/4$ the bigger and $w_2 = \lambda_{sp}/8$ the smaller. Furthermore, as proposed in this work, we are able to make a study of the variation of the frequency response in order to determine the influence of the configuration of the IDT and the piezoelectric material. For this purpose, SAW transducers were designed for the same value of resonance frequency, identical acoustic aperture, number of fingers, and port spacing, but making the necessary variation in the equivalent acoustic wavelength to match the desired frequency. This was done for a single and double finger and also for the SPUDT configuration and for both 128°YX and 64°YX LiNbO3 substrate. With the above, a proper comparison can be made. The design parameters for these sensors are presented in Table 2.

TABLE 2 Parameters for single and double-finger configurations on LiNbO3 128°YX and LiNbO3 64°YX for a SAW transducer working at 97 MHz.

		Single IDT		**Double IDT**		**SPUDT**	
Piezoelectric	**Property**	**Abreviature**	**Value**	**Abreviature**	Value	**Abreviature**	**Value**
128°YX LiNbO3	Finger width	w_s	10 μm	w_d	5 μm	w_{sp}	5, 10 μm
	Acoustic wavelength	λ_s	40 μm	λ_d	40 μm	λ_{sp}	40 μm
	Number of finger pairs	N_s	20	N_d	20	N_{sp}	20
	Acoustic aperture	W_s	4 mm	W_d	4 mm	W_{sp}	4 mm
	Resonance frequency	f_s	97 MHz	f_d	97 MHz	f_{sp}	97 MHz
	Ports separation	l_s	500 μm	l_d	500 μm	l_{sp}	500 μm
64°YX LiNbO3	Finger width	w_s	11.64 μm	w_d	5.82 μm	w_{sp}	11.64, 5.82 μm
	Acoustic wavelength	λ_s	46.58 μm	λ_d	46.58 μm	λ_{sp}	46.58 μm
	Number of finger pairs	N_s	20	N_d	20	N_{sp}	20
	Acoustic aperture	W_s	4 mm	W_d	4 mm	W_{sp}	4 mm
	Resonance frequency	f_s	97 MHz	f_d	97 MHz	f_{sp}	97 MHz
	Ports separation	l_s	500 μm	l_d	500 μm	l_{sp}	500 μm

3 | NUMERICAL SIMULATION METHODOLOGY

To study the design of the SAW transducers, finite element method (FEM) simulations were performed using COMSOL Multiphysics version 6.0. For this purpose, a workflow was used that consists of a) the definitions of the geometrical and physical equations that represent the delta model and those that give sense to the geometry of the SAW transducers. b) the construction of simplified 2D geometry, performed using the parameters described in the previous section for each piezoelectric material and each IDT configuration. c) the configuration of material properties to represent the LiNbO3 128°YX and LiNbO3 64°YX orientations. d) use of additional configurations in the mesh creation in which the finite element sizes are modified. e) addition of appropriate boundary conditions as perfectly matched layers (PML) as artificial domains to avoid unwanted reflections at the edges of the LiNbO3 substrate domain. All configurations were made to improve the simulation process and decrease the computational time, taking advantage of the available hardware, a Corei5, 9th Gen. with 32 GB of RAM. Thus, once simulations were configured, and considering the device as a two-port network, from each simulation performed the IL levels through the input and output ports of the SAW device were extracted.

3.1 | Parameters and global definitions

For the modeling of the SAW transducers, the piezoelectric AC/DC branch was selected, whose module couples both mechanical and electrical physics. First, as global parameters and definitions, the equations and relations defining the resonance frequency, the acoustic wavelength, the velocity, the electromechanical coupling factor, and also the definition of the analytical delta model were written. Then, the global definitions of the boundary conditions were performed. As shown in Figure 3, the lower boundary was selected as a fixed boundary condition and the upper boundary was selected as a free boundary condition, additionally, artificial PML domains were created that subdivide the piezoelectric substrate, to avoid unwanted reflections at the edges of its geometry.

3.2 | Configuration of Materials

The first way to configure the desired material in the created component is to select the default piezoelectric material from the COMSOL material library, and then use an appropriate rotated coordinate system to represent the anisotropy of the selected material through rotation with Euler angles. (0,38,0) for 128°YX and (0,-26,0) for 64°YX LiNbO3 wafers.

Equivalently, material anisotropy representation can be realized by externally calculating the desired elastic, piezoelectric, and permittivity properties of the constitutive piezoelectric equations, using the procedure described in the Auld reference [19] by using the rotation matrix $[M]$ to obtain the desired crystal orientation, for example, the rotation of the stiffness coefficient matrix is realized in (5) where $[c']$ is the desired rotated matrix, and $[c]$ is the original one and the superscript T means the transpose of a matrix.

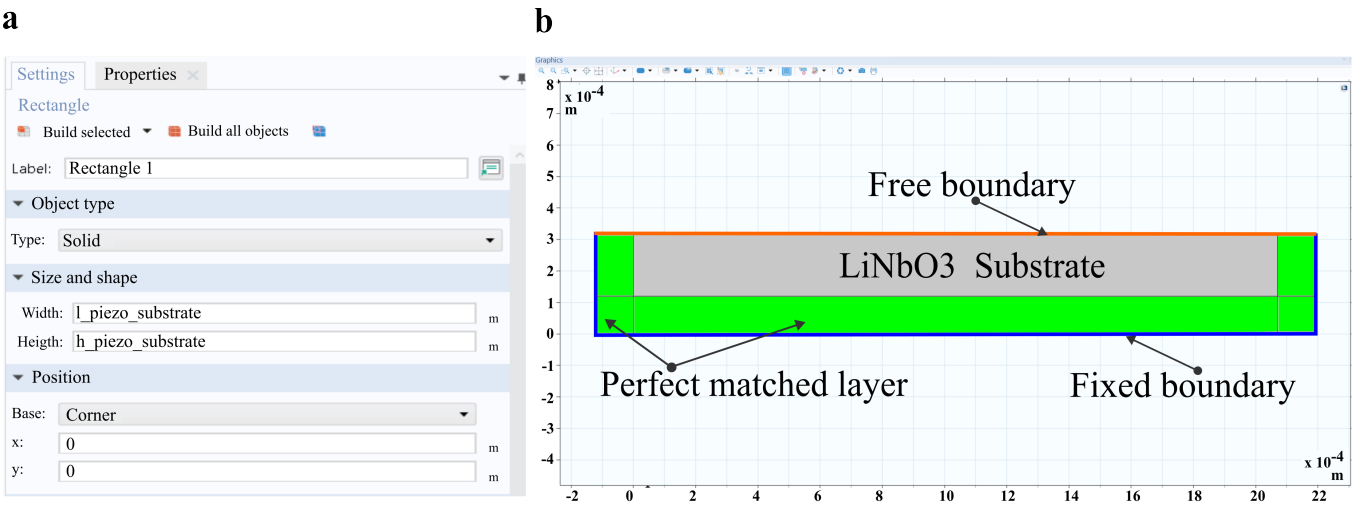

FIGURE 3 2D geometry simplification for complete delay line SAW transducer. a) Parameters of the geometric size of piezoelectric material. b) Geometry of LiNbO3 piezo-substrate where is depicted the use of perfectly matched layers to avoid undesired reflections.

$$[c'] = [M][c][M]^T \tag{5}$$

An equivalent procedure is valid for the missing constants and for any possible rotation.

3.3 | Study and configuration

For each material variant and IDT configuration, a frequency domain study was selected to obtain the S21 parameter of the designed device with a frequency range centered in the resonance frequency f0, from f0-20 MHz to f0+20 MHz, and a frequency step of 100 KHz for a sweep study. The element size of the mesh could be manipulated as depicted in Figure 4 to save time, also other alternatives could be used like using a mapped mesh to define even less finite domains. The results were plotted using a 1D plot group where both the FEM simulation results and the results obtained from the delta model are plotted together, thus comparing their corresponding behaviors.

4 | RESULTS AND DISCUSSION

4.1 | Insertion loss levels for single and double finger IDT on LiNbO3 128°YX and 64°YX

After solving 4.3×10^5 degrees of freedom for the whole model, parameter S21 was first obtained for a single finger configuration where due to its geometrical configuration showed a maximum frequency value of 194 MHz with an insertion loss level at this frequency of $IL(f_0) = -3.6$ dB, and a transition band with an average slope of 12.9 dB/MHz with a clear fit to the theoretical value of the delta model with a Pearson correlation factor (PCF) of $PCF = 0.84$. In comparison, with the double finger configuration, a maximum frequency value of 97 MHz is obtained, with an insertion loss level of $IL(f_0) = -3.3$ dB, an average slope in the transition bands of 23.2 dB/MHz, and a $PCF = 0.82$.

Similarly, with the same number of degrees of freedom simulations were performed for the LiNbO3 64°YX, where the first difference to note is that due to its higher propagation speed, the maximum resonance frequency increases substantially being 226 MHz for single electrode IDT showing an insertion loss level for this frequency of $IL(f_0) = -11.6$ dB, an average slope in the transition band of 17.2 dB/MHz, and a correlation factor with the delta model of $PFC = 0.80$. On the other hand for the dual-electrode configuration, it shows a maximum frequency of 113 MHz, with an insertion loss level $IL(f_0) = -12.1$ dB, an average slope in the transition band of 22.2 dB/MHz, and a correlation factor of $PFC = 0.76$.

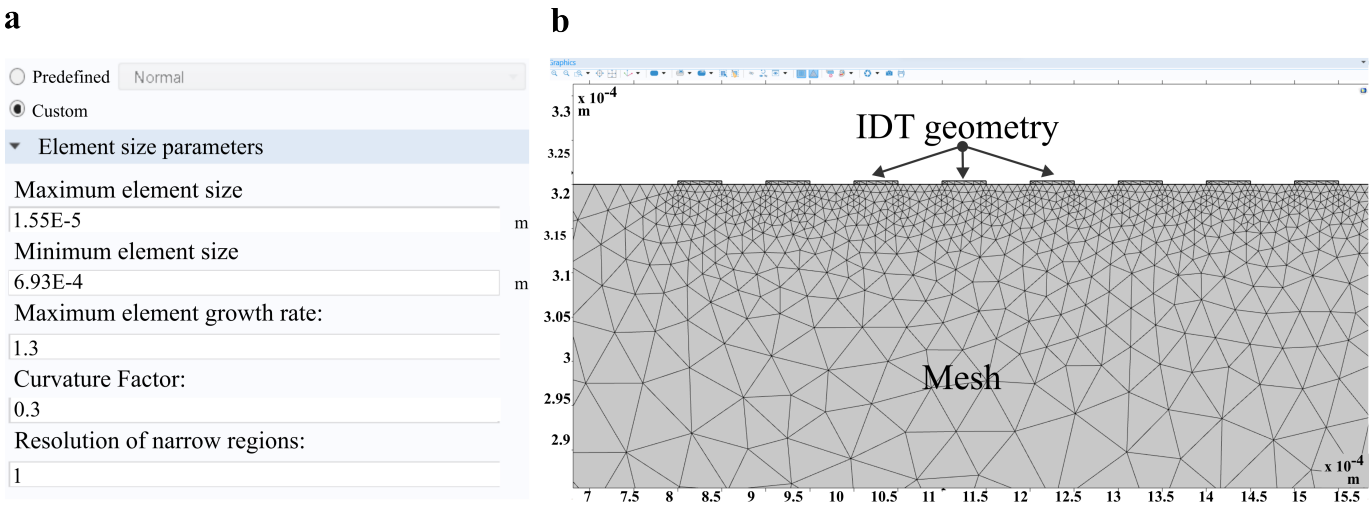

FIGURE 4 Configuration of mesh. a) Parameters of element size in a user-defined mesh geometry, b) Geometry of mesh created where is depicted the IDTs over the piezoelectric surface

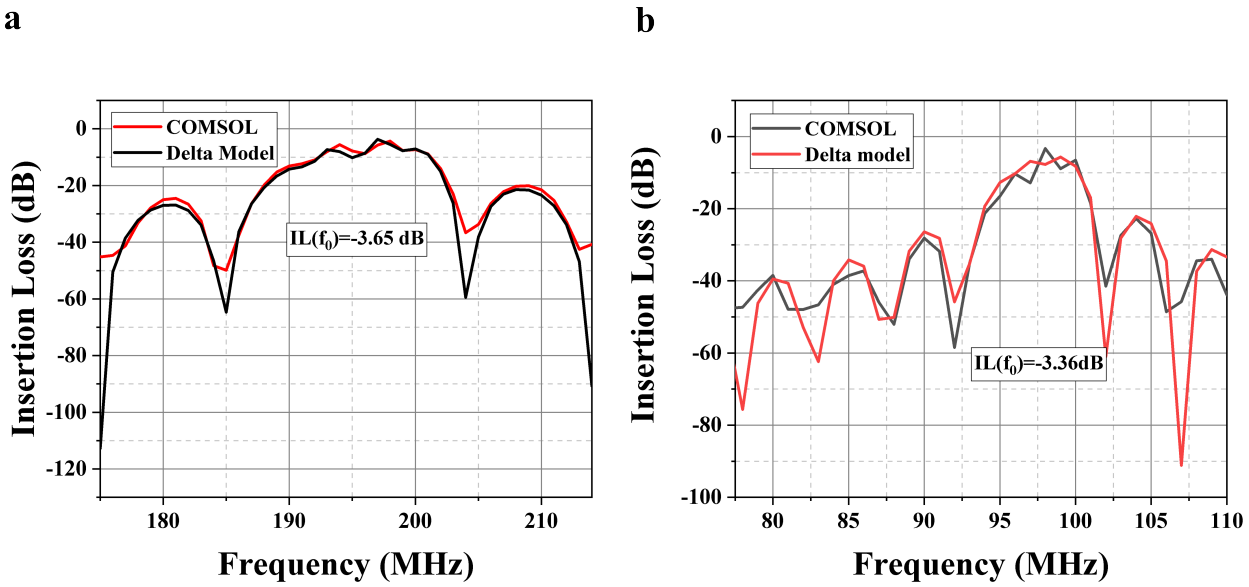

FIGURE 5 Insertion loss levels. a) Single-finger configuration. b) Double-finger configuration for 128°YX LiNbO3

4.2 | Design of a SAW transducer with a particular resonance frequency

Once the validation of the first designs was done, we designed SAW transducers to work at a resonance frequency of 97 MHz, this frequency was selected to be able to compare all the IDT configurations considered, so we start from the fact that in the LiNbO3 128°YX, the maximum frequency obtained is for the double finger configuration, so all the other variations were adjusted to this value. All geometrical parameters corresponding to this design are present in Table 2. In this way we were able to compare the single and double finger configuration and SPUDT for both crystal orientations see Figure 7a. We can observe how the electrical behavior of the SAW transducer is affected by the piezoelectric orientation and the configuration of the IDTs for the same piezoelectric material, for this the data analyzed were: IL levels, average sidelobe levels, and the average slope of the main lobe transition bands in each variation, these results are condensed in Table 3, from which we can observe on the one hand the influence of the change of piezoelectric material from LiNbO3 128°YX to LiNbO3 64°YX comparing the equivalent IDT configurations, with an increase of the insertion loss level: a) it goes from -7. 29 to -11.41 dB for the single-finger configuration.

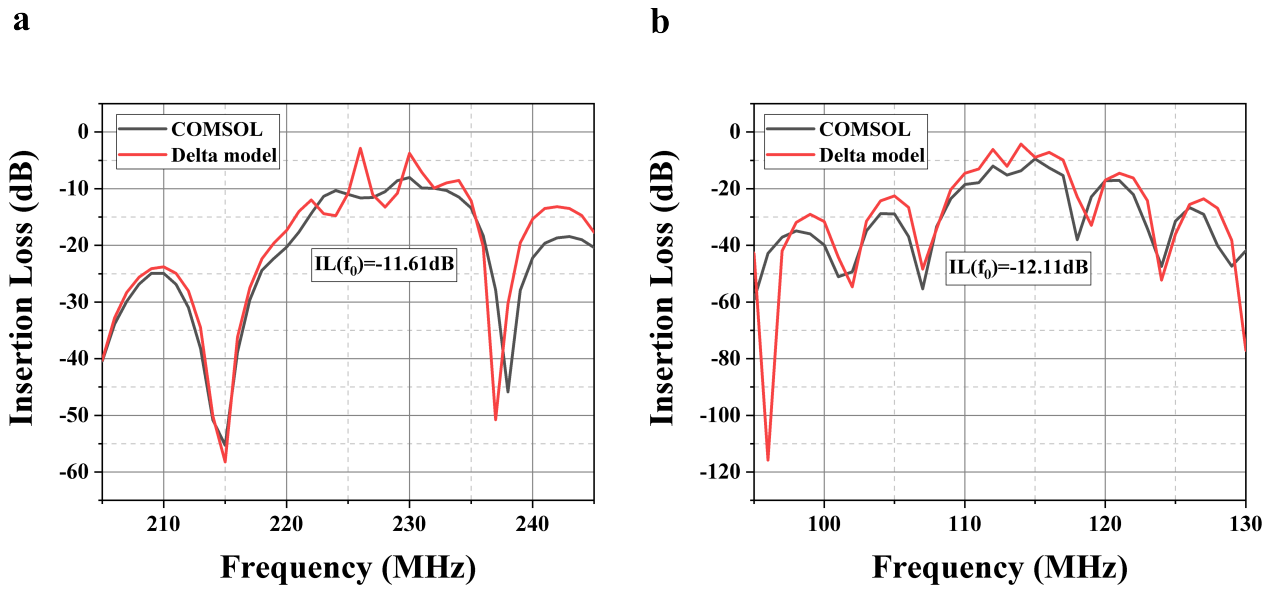

FIGURE 6 Insertion loss levels. a) Single-finger configuration. b) Double-finger configuration for 64°YX LiNbO3

b) it goes from -10.28 to -15.36 dB for the double-finger IDT. c) it goes from -10.76 to -19.41 dB for the SPUDT configuration. Also, a decrease in the mean sidelobe level is observed: a) from 18.63 to 10.06 dB for the single finger IDT. b) from 12.17 to 7.05 dB for the double finger IDT. c) from 17.37 to 6.62 dB for the SPUDT configuration. Different changes are observed in the average slope of the transition band: a) a decrease from 111.59 to 46.95 dB/MHz for the single-finger IDT. b) an increase from 46.96 to 109 dB/MHz for the two-finger IDT. c) a decrease from 54.53 to 48.30 dB/MHz for the SPUDT configuration. On the other hand, the influence of the IDT configuration can be observed by comparing the electrical behavior when changing from single-finger IDT to two-finger IDT to SPUDT configuration in the same piezoelectric material, showing an increase of the insertion loss level: a) changes from -7.29 to -10.28 and -10.76 dB for LiNbO3 128°YX. b) changes from -11.41 to -15.36 and -19.41 dB for LiNbO3 64°YX. Different values of the mean sidelobe level were also observed: a) a non-trending change from 18.63 to 12.17 and 17.37 dB for LiNbO3 128°YX b) a decreasing trend change from 10.06 to 7.05 and 6.62 dB for LiNbO3 64°YX. Different values of the average slope of the transition band are observed: a) a trendless change from 111.59 to 46.96 and 54.53 dB/MHz for LiNbO3 128°YX. b) a trendless change from 46.95 to 109 and 48.30 dB/MHz for LiNbO3 64°YX. Finally, better results are obtained in the single-finger configuration for the LiNbO3 128°YX orientation, because it has better levels for Insertion loss of -7.29 dB, average side lobe level of 18.63 dB, and average slope of the transition band of 111.59 dB/MHz.

TABLE 3 Results obtained for single and double-finger configurations on LiNbO3 128°YX and LiNbO3 64°YX for a SAW transducer working at 97 MHz (the lateral lobe levels were obtained with reference to the level of the main lobe).

		Single IDT	Double IDT	SPUDT
Piezoelectric	**Propertie**			
128°YX LiNbO3	Insertion Loss	-7.29 dB	-10.28 dB	-10.76 dB
	Average side lobe level	18.63 dB	12.17 dB	17.37 dB
	Average slope of transition band	111.59 dB/MHz	43.96 dB/MHz	54.53 dB/MHz
64°YX LiNbO3	Insertion Loss	-11.41 dB	-15.36 dB	-19.41 dB
	Average side lobe level	10.06 dB	7.05 dB	6.62 dB
	Average slope of transition band	46.95 dB/MHz	109 dB/MHz	48.30 dB/MHz

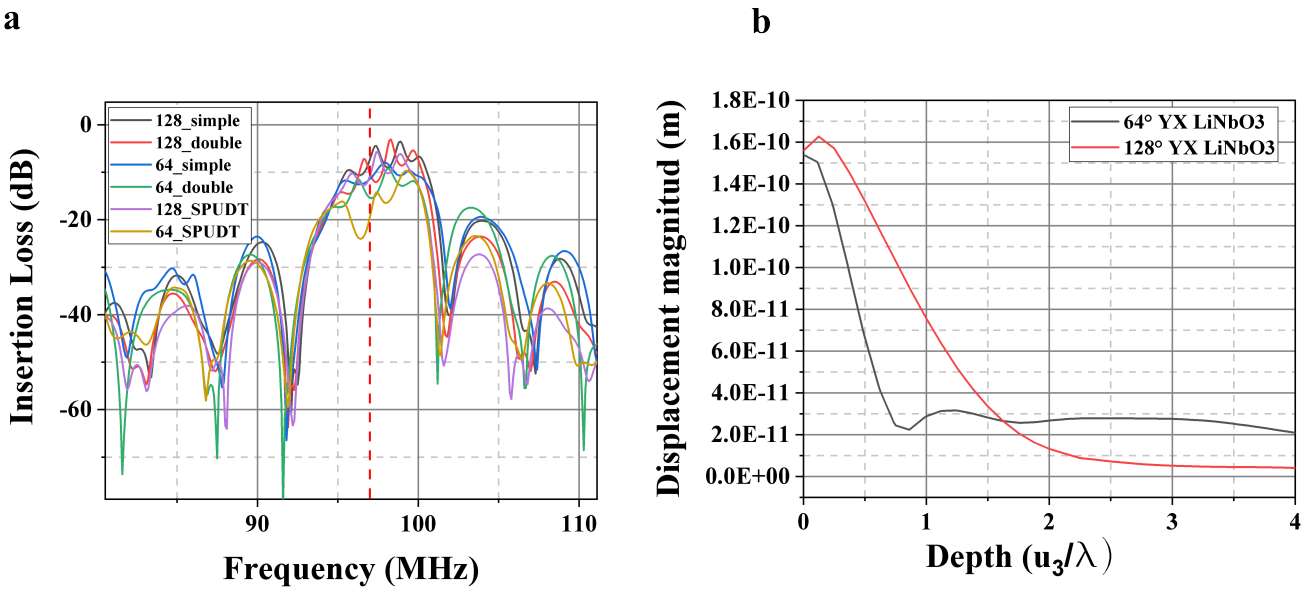

FIGURE 7 Insertion loss levels for a 97 MHz resonance frequency SAW transducer. A comparison of the insertion loss levels could be made for the different IDT configurations and piezoelectric crystal orientations. Displacement magnitude as a function of depht/λ, the length of depth in piezoelectric substrate.

Also from the COMSOL simulation we can extract one of the main characteristics that define the influence of crystal cuts, measuring the displacement magnitude in the center of the SAW transducer delay line as a function of length in the depth of the piezoelectric transducer see Figure 7b, it shows the fact that in 128°YX, having a Rayleigh-type vibration mode the attenuation of displacement decay almost exponentially having a more concentrated influence in the surface of the SAW transducer, which contrasts with the 64°YX orientation having an SH-SAW vibration mode, where the displacement also decay rapidly but maintains a higher value along the depth of piezoelectric substrate.

5 | CONCLUSIONS

Numerical simulation has been shown to be an excellent tool for complementing the design of SAW transducers, we prove their advantages by making an analysis of the influence of the type of piezoelectric substrate and the geometrical configuration of the IDTs on the electrical characteristics of a SAW-type transducer. We observe that the COMSOL numerical simulations show an excellent correlation with the results obtained analytically with the delta model, quantified with a Pearson correlation factor of 0.84, and 0.82 for single and double-finger on LiNbO3 128°YX and a Pearson correlation factor of 0.80 and 0.76 for single and double-finger configuration on LiNbO3 64°YX. Additionally, the numerical simulations were satisfactorily used to model the proposed IDT configurations, giving us the advantage of taking into account physical effects which can be analyzed like the total displacement as a function of the crystal depth in different orientations. Furthermore, the simulation was successfully used to model a SAW transducer working at a particular resonance frequency of 97 MHz, with this design we analyze the influence of the geometrical configuration of the IDTs and the orientation of the piezoelectric substrates, which are mixed in complex way, on the one hand, the orientation of the piezoelectric material determines the propagation velocity, the dielectric permittivity, and the electromechanical coupling factor, and determines the vibration mode of the substrate, we observed from simulation results that 1) changing from 128°YX to 64°YX piezoelectric substrates, for the same IDT configuration, the frequency response change, obtaining larger insertion losses and smaller lateral lobe levels. 2) The desired resonance frequency determines the width of fingers on each configuration of IDT which in turn modifies the frequency response of the SAW transducer. In a similar way, the change from single-finger to double-finger to SPUDT configuration also increases the insertion loss. According to the observed results the best design variant is the one with single fingers in the 128°YX LiNbO3 orientation showing an insertion loss level of -7.29 dB, an average lobe level of 18.63 dB, and 115.59 dB/MHz of average slope in the transition band, this results may be due to the fact that the amount of mass deposited to form the IDTs is lower in the configuration with fewer fingers whose effect is

noticeable in the observed electrical characteristics obtained. On the other hand, in 128°YX orientation, a larger deformation is confined on the surface of the device. Then, the amount of electric potential carried that reaches the output port is much higher, a further study can be extended from this assumption. Finally, this methodology can be applied in the fabrication of SAW transducers, controlling their geometrical properties and electrical behavior, through variations in dimensions for applications in different fields such as electronic filters, ultrasonic transducers, or a wide variety of sensors.

ACKNOWLEDGMENTS

The authors would like to thank the IPN for the use of its facilities, the BEIFI SIP20230389, SIP20230952 SIP20231075 and SIP20231335 projects, and CONAHCYT for its support with postgraduate scholarships.

CONFLICT OF INTEREST

The authors declare no potential conflict of interests.

REFERENCES

1. Cao L, Yan J, Yin L. Effects of dielectric substrates on piezoelectric transducer tunable filter. *Microwave and Optical Technology Letters.* 2019;61(10):2399–2404.
2. Ye J, LETCHER SV, RAND AG. Piezoelectric biosensor for detection of Salmonella typhimurium. *Journal of food science.* 1997;62(5):1067–1086.
3. Kim Y, Lee J, Hong H, Park S, Ryu W. Self-Powered Wearable Micropyramid Piezoelectric Film Sensor for Real-Time Monitoring of Blood Pressure. *Advanced Engineering Materials.* 2023;25(2):2200873.
4. Pohl A. A review of wireless SAW sensors. *IEEE transactions on ultrasonics, ferroelectrics, and frequency control.* 2000;47(2):317–332.
5. Liew K, He X, Ng T, Kitipornchai S. Active control of FGM shells subjected to a temperature gradient via piezoelectric sensor/actuator patches. *International journal for numerical methods in engineering.* 2002;55(6):653–668.
6. Lee S, Kim D, Lee S, et al. Ambient humidity-induced phase separation for fiber morphology engineering toward piezoelectric self-powered sensing. *Small.* 2022;18(17):2105811.
7. Wang YL, Shih JS. Multi-Channel Piezoelectric Crystal Gas Sensor with Principal Component Analysis for Organic Solvent Pollutants from Polymer Plants. *Journal of the Chinese Chemical Society.* 2006;53(6):1427–1437.
8. Fu YQ, Luo J, Nguyen NT, et al. Advances in piezoelectric thin films for acoustic biosensors, acoustofluidics and lab-on-chip applications. *Progress in Materials Science.* 2017;89:31–91.
9. Hoang T, Beghi M. SAW parameters analysis and equivalent circuit of SAW device. *Acoustic Waves-From Microdevices to Helioseismology.* 2011:443–483.
10. Jesus RC, Carvalho EA, Tamarin O, Freire RC, Dejous C. Equivalent circuit models for SAW delay line sensors. *IEEE Sensors Journal.* 2022;22(12):11810–11818.
11. Moustafa M, Laouini G, ElNaggar M, AlZoubi T. Investigation into surface acoustic wave sensor for DCM gas detection using COMSOL multiphysics. *Ferroelectrics.* 2021;572(1):94–105.
12. Zhang L, Su HH, Tong MS. A novel design of surface acoustic wave-based chipless radio frequency identification tag based on multiphysics modeling. *International Journal of Numerical Modelling: Electronic Networks, Devices and Fields.* 2021;34(6):e2857.
13. Hribšek MF, Ristić SS, Radojković BM, Filipović ZL, Ristić OR. Modelling of chemical surface acoustic wave sensors and comparative analysis of new sensing materials. *International Journal of Numerical Modelling: Electronic Networks, Devices and Fields.* 2013;26(3):263–274.
14. Morgan D. *Surface acoustic wave filters: With applications to electronic communications and signal processing*. Academic Press, 2010.
15. Mandal D, Banerjee S. Surface acoustic wave (SAW) sensors: Physics, materials, and applications. *Sensors.* 2022;22(3):820.
16. Cole M, Sehra G, Gardner JW, Varadan VK. Development of smart tongue devices for measurement of liquid properties. *IEEE Sensors Journal.* 2004;4(5):543–550.
17. Soluch W. Design of SAW delay lines for sensors. *Sensors and Actuators A: Physical.* 1998;67(1-3):60–64.
18. Hashimoto Ky, Hashimoto KY. *Surface acoustic wave devices in telecommunications*. 116. Springer, 2000.
19. Auld BA. *Acoustic fields and waves in solids*. Ripol Classics, 1973.
20. Rocha-Gaso MI, March-Iborra C, Montoya-Baides Á, Arnau-Vives A. Surface generated acoustic wave biosensors for the detection of pathogens: A review. *Sensors.* 2009;9(7):5740–5769.
21. Le TT, Curry EJ, Vinikoor T, et al. Piezoelectric nanofiber membrane for reusable, stable, and highly functional face mask filter with long-term biodegradability. *Advanced Functional Materials.* 2022;32(20):2113040.
22. Zhuoyun N, Yijing M, Ruijuan L, Dongsheng G. Improved disturbance rejection control for piezoelectric actuators based on combination of ESO and Q-filter. *Electronics Letters.* 2018;54(14):872–874.